jbc The Journal of Biological Chemistry
AFFINITY SITES
ASBMB American Society for Biochemistry and Molecular Biology

Cell Biology:

Biochemical Characterization of the Bi-lobe Reveals a Continuous Structural Network Linking the Bi-lobe to Other Single-copied Organelles in *Trypanosoma brucei*

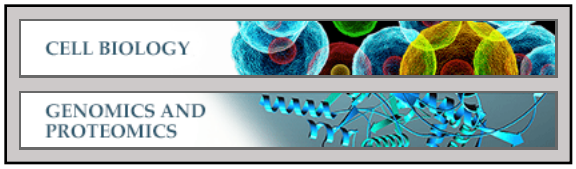

Ladan Gheiratmand, Anais Brasseur, Qing Zhou and Cynthia Y. He

J. Biol. Chem. 2013, 288:3489-3499.
doi: 10.1074/jbc.M112.417428 originally published online December 12, 2012

Access the most updated version of this article at doi: 10.1074/jbc.M112.417428

Find articles, minireviews, Reflections and Classics on similar topics on the JBC Affinity Sites.

Alerts:
- When this article is cited
- When a correction for this article is posted

Click here to choose from all of JBC's e-mail alerts

Supplemental material:
http://www.jbc.org/content/suppl/2012/12/12/M112.417428.DC1.html

This article cites 45 references, 21 of which can be accessed free at
http://www.jbc.org/content/288/5/3489.full.html#ref-list-1

Downloaded from http://www.jbc.org/ at UNIV BORDEAUX on February 5, 2015

THE JOURNAL OF BIOLOGICAL CHEMISTRY VOL. 288, NO. 5, pp. 3489–3499, February 1, 2013
© 2013 by The American Society for Biochemistry and Molecular Biology, Inc. Published in the U.S.A.

Biochemical Characterization of the Bi-lobe Reveals a Continuous Structural Network Linking the Bi-lobe to Other Single-copied Organelles in *Trypanosoma brucei*[*][S]

Received for publication, September 7, 2012, and in revised form, November 20, 2012 Published, JBC Papers in Press, December 12, 2012, DOI 10.1074/jbc.M112.417428

Ladan Gheiratmand[1], **Anais Brasseur, Qing Zhou, and Cynthia Y. He**[2]

From the Department of Biological Sciences, Centre for BioImaging Sciences, National University of Singapore, 14 Science Drive 4, Singapore 117543

Background: The bi-lobe is a structure critical to biogenesis and inheritance of several single-copied organelles in *Trypanosoma brucei*.
Results: The bi-lobe was immunoisolated, and new bi-lobe associated proteins were characterized.
Conclusion: A continuous structural network connected bi-lobe to other organelles in *Trypanosoma brucei*.
Significance: Structural tethering may be a general strategy to ensure orderly and faithful inheritance of single-copied organelles in protists.

***Trypanosoma brucei,* a unicellular parasite, contains several single-copied organelles that duplicate and segregate in a highly coordinated fashion during the cell cycle. In the procyclic stage, a bi-lobed structure is found adjacent to the single ER exit site and Golgi apparatus, forming both stable and dynamic association with other cytoskeletal components including the basal bodies that seed the flagellum and the flagellar pocket collar that is critical for flagellar pocket biogenesis. To further understand the bi-lobe and its association with adjacent organelles, we performed proteomic analyses on the immunoisolated bi-lobe complex. Candidate proteins were localized to the flagellar pocket, the basal bodies, a tripartite attachment complex linking the basal bodies to the kinetoplast, and a segment of microtubule quartet linking the flagellar pocket collar and bi-lobe to the basal bodies. These results supported an extensive connection among the single-copied organelles in *T. brucei*, a strategy employed by the parasite for orderly organelle assembly and inheritance during the cell cycle.**

Faithful duplication and segregation of subcellular organelles is an essential component of the eukaryotic cell cycle. Molecular mechanisms that allow orderly organelle inheritance are increasingly evident in animal, plant, yeast, and other eukaryotic cells (1–4). Depending on the morphology, copy number, and biological functions, different organelles may employ different mechanisms to ensure faithful replication and partitioning into dividing cells. However, cytoskeletal components, such as actins and microtubules, are critically involved in precise positioning and inheritance of many organelles (5). *Trypanosoma brucei* is a protozoan parasite responsible for human African sleeping sickness. It has a complex life cycle including a bloodstream form that proliferates in the mammalian host and a procyclic form that resides in the midgut of the insect vector, tse-tse fly. Each procyclic *T. brucei* cell contains a single nucleus, a single pair of basal bodies, a single Golgi and associated ER[3] exit site, and a single reticulated mitochondrion that harbors a single aggregate of kinetoplast DNA. A single flagellum is nucleated by the mature basal body. The flagellum exits from the flagellar pocket and remains attached to the cell body through membrane adhesion proteins and an intracellular flagellum attachment zone (FAZ) complex that contains electron dense protein filament and a set of four microtubules known as the microtubule quartet (MtQ) (6, 7). The exact positioning and inheritance of these organelles/structures during the cell cycle are tightly regulated by a complex microtubule network and other cytoskeletal elements in the parasite (8, 9), whereas actin has little effect (10, 11). During the cell cycle, immediately after basal body duplication, a new flagellum and a new FAZ is assembled posterior to the "old" structures. The coordinated elongation of the new flagellum-FAZ complex powers the basal body segregation (12, 13), which in turn drives kinetoplast division (14). The latter process is mediated by a tripartite attachment complex (TAC) that physically tethers the kinetoplast DNA to the basal bodies (15). Depletion of the TAC component p166 severed the basal body-kinetoplast connection, leading to asymmetric segregation of the kinetoplast DNA (16). Basal body movement is also crucial for the division of membrane organelles, such as the flagellar pocket (17), the ER exit site, and Golgi apparatus (18). Biogenesis of the flagellar pocket requires BILBO1, a structural component of the FPC (19). ER exit site/Golgi duplication and segregation, on the other hand, depend on a bi-lobed structure initially identified by centrin staining at the proximal base of the flagellum near the flagellar pocket (18, 20, 21).

[*] This work was supported by the Singapore National Research Foundation.
[S] This article contains supplemental Tables S1 and S2 and Figs. S1–S6.
[1] A recipient of the A*STAR SINGA fellowship.
[2] To whom correspondence should be addressed. Tel.: 65-65167377; Fax: 65-65167203; E-mail: dbshyc@nus.edu.sg.

[3] The abbreviations used are: ER, endoplasmic reticulum; FAZ, flagellum attachment zone; MtQ, microtubule quartet; FPC, flagellar pocket collar; PFR, paraflagellar rod; TAC, tripartite attachment complex; Spef1, sperm flagellar protein1; BRCT, BRCA1 C terminus; DIC, differential interference contrast; PFA, paraformaldehyde.

Downloaded from http://www.jbc.org/ at UNIV BORDEAUX on February 5, 2015

In addition to centrins, TbMORN1 and TbLRRP1 (22, 23) both are present at the bi-lobe but over a region distinct to that labeled with centrin (24). Depletion of TbLRRP1 led to inhibited duplication of the Golgi, the FPC, and the FAZ as well as inhibited basal body segregation and cell division (23). These findings emphasized the structural complexity of the bi-lobe and its association with other cytoskeletal structures. To further understand the bi-lobe and its associated structures, we performed proteomic analyses on immunoisolated bi-lobes. Because the immunoisolation was performed in isotonic buffers without any detergent, both cytoskeletal and soluble components were preserved in the bi-lobe fraction. Subcellular localization and functional characterization of candidate proteins revealed an extensive association of the bi-lobe with other cytoskeletal and membrane-bound organelles in the flagellar pocket region, which was crucial for the orchestrated organelle biogenesis and inheritance during the cell cycle.

EXPERIMENTAL PROCEDURES

Cell Lines and DNA Constructs—Procyclic 29.13 *Trypanosoma brucei brucei* cells (25) used in this study were maintained at 28 °C in the Cunningham medium containing 15% heat-inactivated, tetracycline-free fetal calf serum (Clontech). Bloodstream single marker cells (25) were maintained in HMI-9 medium containing 10% heat-inactivated, tetracycline-free fetal calf serum (Clontech) at 37 °C in an incubator containing 5% CO_2.

Full-length coding sequence of TbSpef1 (Tb927.4.3130) was amplified and fused to the N terminus of the YFP tag in pXS2 vector (18, 26). p197 (Tb927.10.15750) and BB50 (Tb927.4.3440) were endogenously tagged with YFP at their N termini using a modified pCR4Blunt-TOPO vector (22). A cell line that allowed stable expression of YFP-TbLRRP1 from an endogenously replaced allele was previously described (23). Inducible overexpression of YFP-FP45 (Tb927.9.9730) was achieved using a pLew100 plasmid (25). RNAit, an automated web-based tool (27), was used to select a 485-bp fragment in TbSpef1 (nucleotides167–651), a 410-bp fragment in p197 (nucleotides 2672–3082), and a 406-bp fragment in FP45 (nucleotides 5–411), which were cloned into the pZJM plasmid (28) for TbSpef1-RNAi, p197-RNAi, and FP45-RNAi, respectively. Stable cell transfections were achieved by electroporation with 15 μg of linearized plasmid followed with serial dilution and selection with appropriate drugs.

Antibodies—Full-length coding sequence of TbSpef1 and FP45 were expressed as His-tagged fusions in *Escherichia coli*. Affinity-purified His-FP45 was then used to inject rats for polyclonal antibody production. Affinity-purified His-Spef1 was treated with thrombin to remove the His tag and then injected into rabbits for polyclonal antibody production. Purified IgG from each serum was used for Western blotting, immune fluorescence, and immuno electron microscopy where mentioned in the text.

Immunofluorescence Microscopy—Procyclic or bloodstream form cells were washed and resuspended in phosphate-buffered saline (PBS, pH7.4), attached to coverslips, and fixed and permeabilized with cold methanol (−20 °C) or 4% PFA followed with 0.25% Triton X-100 where mentioned. For extracted cytoskeletons, cells attached to coverslips were incubated with PEM (100 mM PIPES, 1 mM EGTA, 1 mM $MgSO_4$, pH 6.9) containing 1% Nonidet P-40 with or without 1 M NaCl at room temperature for 5 min. The extracted cytoskeletons were then fixed with 4% PFA. Fixed samples were then blocked with 3% BSA in PBS and probed with the corresponding antibodies. Primary antibodies used in this study were anti-TbLRRP1 (23) to mark the bi-lobe, anti-CC2D (29) and L3B2 for the FAZ (30), anti-BILBO1 for the FPC (19), anti-TbCentrin4 for basal bodies and bi-lobe (21), anti-PAR (31) or anti-PFR1[4] for the paraflagellar rod along the flagellum and YL1/2 for the basal bodies (AbCam). Nuclear and kinetoplast DNA were stained with 10 μg/ml DAPI for 20 min. Labeling of bloodstream form cells with Texas Red-labeled tomato-lectin (Vector Laboratories) was performed at 37 °C for 20 min. Cells were then fixed with 4% PFA and permeabilized with 0.1% Triton X-100 before immunolabeling with anti-FP45. Images were acquired using a Zeiss Axio Observer microscope equipped with a 63XNA1.4 objective and a CoolSNAP HQ2 CC2D camera (Photometrics). The super-resolution images were acquired by a Zeiss ELYRA system equipped with a 63× Plan-Apochromatic 1.4NA and an Andor iXon DU 885 EMCCD for the SR-SIM images. Adobe photoshop was used for processing images.

Immunoisolation of Bi-lobe—100 ml log phase YFP-TbLRRP1 cells (with YFP-TbLRRP1 expressed from an endogenous allele) were harvested by centrifugation at 1800 × *g* for 10 min and washed twice in 50 and 25 ml of lysis buffer H (250 mM sucrose, 50 mM Hepes-KOH, pH 7.4, 4 mM $MgCl_2$). Cells were then resuspended in 1 ml of cold buffer H supplemented with protease inhibitor mixture (Roche Applied Science) and 1 mM PMSF. Parasite suspension was then sonicated for a total of 12 s (6 cycles of 2 s sonication followed with 10 s rest) at 80% amplitude (Sonics-Vibracell, 130W). The efficiency of the homogenization and integrity of the bi-lobe was monitored by microscopy. After homogenization, cell lysates were centrifuged at 2500 × *g* for 5 min at 4 °C to remove unbroken cells and large cell debris. The supernatant was treated with DNase I on ice for 30 min. To immunoisolate the YFP-labeled bi-lobe, 100 μl of protein G-conjugated magnetic beads (Dynabeads, Invitrogen) were coated with anti-GFP by incubating in the antibody for 30 min at room temperature. After extensive washes with PBS containing 0.05% Tween 20, the anti-GFP-coated beads were added to the DNase I-treated supernatant and incubated for 4 h at 4 °C with gentle mixing. After extensive washes with buffer H, the magnetic beads were examined by fluorescence microscopy to monitor bi-lobe binding (Fig. 1*B*). Proteins bound to the beads were eluted by boiling in gel loading buffer containing 1% SDS, fractionated on 12% SDS-PAGE, and processed for silver staining and immunoblotting (supplemental Fig. S1). Parasites expressing YFP only were processed at the same time as above and used as negative controls. For further mass spectrometry analyses, gel regions containing the specific bands (*arrows*, Fig. 1*D*) were excised, trypsinated, and vacuum-dried.

LC/MS-MS and Data Analysis— 0.1% formic acid was used to reconstitute the dried peptides. Peptides were then analyzed

[4] L. Gheiratmand, A. Brasseur, Q. Zhou, and C. Y. He, unpublished results.

Downloaded from http://www.jbc.org/ at UNIV BORDEAUX on February 5, 2015

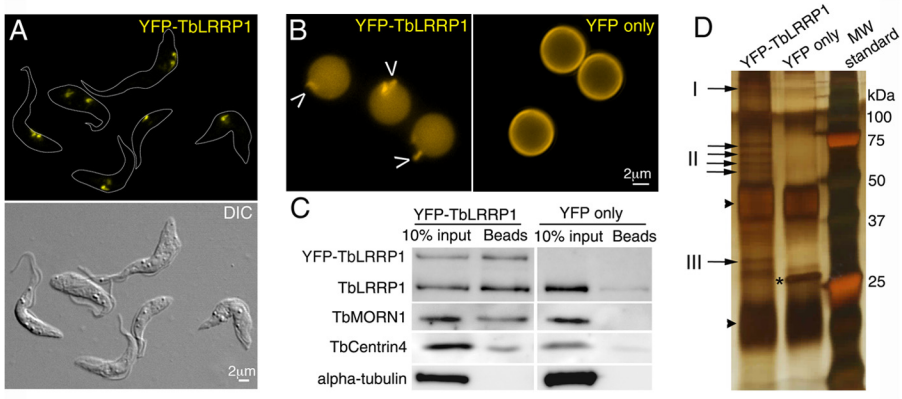

FIGURE 1. **Immunoisolation of YFP-TbLRRP1-labeled bi-lobe.** *A*, procyclic *T. brucei* cells endogenously expressing YFP-TbLRRP1 were fixed with 4% PFA. The YFP-labeled, looped structures represented the bi-lobes during different cell cycle stages. Parasite cells were demarcated with *gray lines*. *B*, shown are fluorescence images of magnetic beads bound to the bi-lobe complex (*arrowheads*) immunoisolated from YFP-TbLRRP1 cell lysates. Beads incubated with YFP cell lysates were used as the negative control. *C*, immunoblotting analyses of the immunoisolated bi-lobe fraction are shown. Known bi-lobe proteins TbLRRP1 (both YFP-TbLRRP1 and endogenous TbLRRP1), TbMORN1, and TbCentrin4 were all specifically detected in the immunoisolated products from YFP-TbLRRP1 lysates but not in the YFP control. α-Tubulin, however, was not detectable in the bi-lobe fraction. *D*, proteins eluted from anti-GFP coated beads were fractionated by 12% SDS-PAGE, and the gel was processed for silver staining. Whereas the control beads incubated with YFP cell lysates precipitated YFP efficiently (~28-kDa band indicated by the *asterisk*), beads incubated with YFP-TbLRRP1 lysate pulled down several specific bands (indicated by the *arrows*) that were excised and processed for LC/MS-MS. Two heavily stained bands marked by the *arrowheads* represented the heavy and light chains of the anti-GFP antibody and were found in both YFP-TbLRRP1 and YFP-only lanes.

by an LTQ-FT ultra mass spectrometer (Thermo Fisher Scientific) and a Prominence™ HPLC unit. Before re-equilibrating the column at 5% buffer B for 8 min, a 90-min gradient was established using mobile phase buffer A (0.1% formic acid in H_2O) and buffer B (0.1% formic acid in acetonitrile). The gradient began with a ramp from 5 to 30% B followed by 50% B and a ramp from 50 to 80% B for 66, 10, and 4 min, respectively. HPLC was operated at a constant flow rate of 20 μl/min and ~300 nl/min at the electrospray emitter (Michrom BioResources). An ADVANCE™ CaptiveSpray™ Source (Michrom BioResources) with an electrospray potential of 1.5 kV was used to ionize the samples. Data acquired by LTQ-FT ultra in the positive ion mode were used to perform a full MS scan at a resolution of 100,000 and a maximum ion accumulation time of 1000 ms. For collecting peptides and measuring their fragments generated by CID, a linear ion trap with the default AGC was used. All MS/MS spectra were searched for protein identifications against *T. brucei* GeneDB using Mascot (version 2.2.07, Matrix Science, Boston, MA) search engines.

Immunoelectron Microscopy—Immunogold labeling was performed on cytoskeletons extracted with 1% Nonidet P-40 and 1 M NaCl as previously described (29) with minor modifications. Briefly, 10^7 cells were harvested, washed with PBS, and attached to carbon Formvar-coated nickel grids (EMS). Cells were extracted in PEM buffer containing 1% Nonidet P-40 and 1 mM NaCl for 30 min at room temperature. The extracted cytoskeletons were washed with PEM, fixed with 2.5% glutaraldehyde, neutralized with 100 mM glycine, blocked with 1% BSA, and labeled with anti-TbSpef1 (1:200). Goat-anti-rabbit IgG conjugated to 10-nm gold particles (EMS) was used at 1:100 dilution where little background labeling was observed. The labeled grids were washed, fixed again with 2.5% glutaraldehyde, and stained briefly in a drop of 0.5% aurothioglucose prepared in distilled, deionized H_2O. After air dry, grids were observed and imaged by a JEOL 1200 EX electron microscope.

For immuno-cryoEM, procyclic cells induced for YFP-FP45 expression were fixed with 4% paraformaldehyde and 0.2% glutaraldehyde in 100 mM phosphate buffer, pH 7.2, for 1 h at 4 °C. Samples were then embedded in 10% gelatin and infiltrated overnight with 2.3 M sucrose, 20% polyvinyl pyrrolidone in PIPES with $MgCl_2$ at 4 °C. After getting trimmed and frozen in liquid nitrogen, samples were sectioned and probed with anti-GFP followed by the gold-conjugated secondary antibody (Jackson ImmunoResearch Laboratories, West Grove, PA). Sections were then washed in PIPES buffer, rinsed with water, stained with 0.3% uranyl acetate and 2% methyl cellulose and observed with a JEOL 1200 EX electron microscope.

RESULTS

Immunoisolation of the Bi-lobe and Associated Structures—TbLRRP1 is a bi-lobe resident, leucine-rich repeat containing protein previously identified through a comparative proteomic analysis (23). Although the molecular mechanism is not yet clear, TbLRRP1 is important for proper duplication and segregation of the bi-lobe and adjacent FPC, Golgi, and FAZ. The exclusive presence of TbLRRP1 on the bi-lobe also makes it an excellent marker for bi-lobe purification.

Procyclic cells with one endogenous TbLRRP1 allele stably replaced with YFP-TbLRRP1 showed distinct labeling of the bi-lobe as one or two looped structures in each live parasite (Fig. 1*A*) (23). These cells were homogenized by sonication in an isotonic buffer free of detergent, and the resulting cell lysates were incubated with anti-GFP coated Dynabeads for immunoisolation of the YFP-labeled bi-lobes (supplemental Fig. S1; Fig. 1*B*). Lysates of cells expressing YFP only were used as a negative control. By fluorescence microscopy, YFP-labeled structures ~1 μm long could be observed on anti-GFP-beads incubated with YFP-TbLRRP1 cell lysates but not on beads incubated with YFP cell lysates (Fig. 1*B*). By immunoblotting analyses, several known bi-lobe markers including TbLRRP1 (both YFP-

Downloaded from http://www.jbc.org/ at UNIV BORDEAUX on February 5, 2015

TbLRRP1 and endogenous TbLRRP1), TbMORN1, and TbCentrin4 were specifically detected in the bi-lobe isolates from the YFP-TbLRRP1 cells. α-Tubulin, however, was not enriched in the bi-lobe fraction (Fig. 1*C*). Furthermore, silver staining of the bi-lobe fraction revealed several specific protein bands that were not found in the YFP control (*arrows*, Fig. 1*D*). Gel regions containing these bands were excised, trypsinated, and analyzed using LC/MS-MS. Proteins identified in individual excised bands were then categorized into three groups based on their molecular weights. Group I contained proteins ~100–250 kDa, group II contained proteins ~55–75 kDa, and group III contained proteins ~30–35 kDa in size (Fig. 1*D*; supplemental Table S1).

Identification of Bi-lobe-associated Proteins by LC/MS-MS—A total of 74 proteins were identified as a result of two independent immunoisolation and MS assays. Of these, 44 proteins that had at least 2 matching peptides were listed in supplemental Table S1. The bi-lobe protein TbLRRP1 was identified with a high hit number, validating the immuno-isolation approach. The FPC marker BILBO1 was also identified with high confidence, agreeing with previous reports that BILBO1 co-purified with the bi-lobe in detergent/salt-extracted flagellar complex (19, 23). Bi-lobe proteins TbCentrin2 and TbCentrin4 are small molecular weight proteins that migrate to the lower part of the gel that was not selected for MS analyses. The other known bi-lobe protein TbMORN1 (~41 kDa) was likely masked by anti-GFP heavy chain (Fig. 1*D*) and also was not analyzed by MS.

As shown in supplemental Table S1, 10 of the 44 high confidence candidates were previously uncharacterized hypothetical proteins. Of the remaining 34, 18 were verified or predicted mitochondrial proteins, suggesting an association between the bi-lobe and the mitochondrion, which harbors the kinetoplast DNA. Several cytoskeletal components were also identified. These included the paraflagellar rod (PFR) proteins PFR1 and PFR2, which form the paraflagellar crystalline tightly associated with the flagellum axoneme (32). The presence of these PFR proteins together with two microtubule-associated proteins is consistent with the tight association between the bi-lobe and the cytoskeletal components, particularly the flagellum, as previously reported by biochemical and ultrastructural analyses (22–24). Other proteins, including two glycosomal proteins, one nuclear pore protein, and an ER luminal protein BiP, were also identified in this dataset. It remained to be investigated if these represented true organelle association or contamination by these abundant proteins.

Based on protein size and bioinformatics prediction of functional domains and cellular localization, seven hypothetical proteins and a previously identified protein, TbSpef1, representing protein candidates from all three groups (highlighted in *red* in supplemental Table S1), were further characterized by stable expression of YFP-tagged proteins (supplemental Table S2). Four of the eight candidates characterized showed no specific cellular localization and were not further pursued. Tb927.4.3440 encoded a previously uncharacterized, ~50-kDa protein that was localized to a pair of bright dots at the base of each flagellum (supplemental Fig. S2A). One dot colocalized precisely with the mature basal body marker YL1/2 (33) (*insets*, supplemental Fig. S2A). Immunogold labeling of detergent and salt-extracted cytoskeleton confirmed its presence on both the mature and pro-basal bodies (supplemental Fig. S2*B*). The protein coded by Tb927.4.3440 was hence named BB50. The other three candidates, p197 (encoded by Tb927.10.15750), FP45 (encoded by Tb927.9.9730), and TbSpef1 (encoded by Tb927.4.3130), were mapped, respectively, to TAC, flagellar pocket, and the MtQ region linking the basal bodies to the bi-lobe, revealing a continuous network linking membrane and cytoskeletal organelles in the flagellar pocket region.

TbSpef1 Localizes to the MtQ Region between the Basal Bodies and the Bi-lobe—Sperm flagellar protein1 (Spef1), also known as CLAMP, was initially identified as a conserved component of motile flagella from mammals to protozoa (34). Spef1/CLAMP interacts with microtubules through a calponin homology domain and thus promotes microtubule bundling and microtubule stabilization (35). In *T. brucei,* a single Spef1 homolog (also known as TbCMF18) is present. RNAi depletion of this protein in both procyclic and bloodstream stages is lethal, causing flagellum detachment, severe flagellum motility defects, and cytokinesis arrest (36, 37). Although thought to be a flagellar component, the exact localization of TbSpef1 was not yet investigated in *T. brucei*. As shown in Fig. 2, stably expressed YFP-TbSpef1 labeled a curved structure in between the kinetoplast and the nuclear DNA, with one end adjacent to the kinetoplast and the other end extending anterior to the proximal base of the FAZ (Fig. 2*A*). This localization and the curved and sometimes hook-like morphology were reminiscent of the bi-lobed structure marked by TbMORN1 and TbLRRP1. Further colocalization studies showed that YFP-TbSpef1 did not colocalize with TbLRRP1 (Fig. 2*B*). Instead, the TbSpef1-containing structure was located further posterior, with the anterior tail passing through/next to the TbLRRP1-labeled loop and the BILBO1-labeled FPC ring (Fig. 2, *B* and *C*). This labeling pattern was confirmed using a polyclonal antibody specific to TbSpef1 (supplemental Fig. S3). Similar to YFP-TbSpef1, anti-TbSpef1 labeled a curved structure with the posterior end overlapping with the TbCentrin4-labeled basal bodies and the anterior tail extending toward the posterior region of the bi-lobe (Fig. 3*A*) that is tightly associated with the FPC. The formation of a new TbSpef1-labeled MtQ occurred early in the cell cycle, before the duplication of the basal bodies (Fig. 3*A*), and this is consistent with the previously observed three-dimensional electron tomographic reconstruction of the flagellar pocket region (17). The relative position of the new TbSpef1-labeled MtQ to the old MtQ (posterior or anterior) could not be reliably distinguished due to the random placing of extracted cells on the coverslips. Under electron microscope (Fig. 3*B*), TbSpef1 (immunogold labeled using anti-TbSpef1) was found along the MtQ track that was nucleated between the mature and pro-basal bodies and extended through or next to the FPC ring. No TbSpef1 labeling was observed, however, on the MtQ anterior to the bi-lobe at any time of the cell cycle (Figs. 2 and 3). Previous functional analyses of TbSpef1 emphasized its effect on flagellum motility and cell division (36, 37). To further understand the function of TbSpef1 as an MtQ-associated protein between the basal bodies and the FPC/bi-lobe, the effects of TbSpef1-RNAi were re-examined in the procyclic cells, with a particular focus on the duplication/segregation of adjacent

Downloaded from http://www.jbc.org/ at UNIV BORDEAUX on February 5, 2015

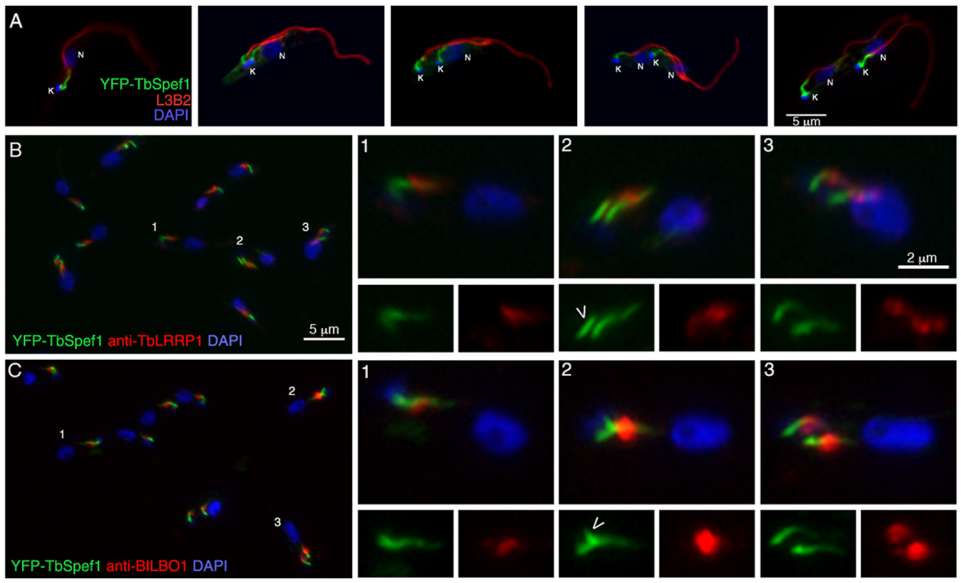

FIGURE 2. **YFP-TbSpef1 localization during the cell cycle.** Cells stably overexpressing YFP-TbSpef1 (*green*) were extracted with 1% Nonidet P-40, fixed with PFA, and probed with L3B2 for FAZ (*A*), anti-TbLRRP1 for the bi-lobe (*B*), or anti-BILBO1 for the FPC (*red*) (*C*). All cells were also stained with DAPI to label the kinetoplast (*small blue dot marked with K* in *A*) and the nucleus (*large blue structure marked with N* in *A*). YFP-TbSpef1 labeled a curved and sometimes hook-like structure with one end adjacent to the kinetoplast and the other end extending anterior to the initiating base of the FAZ (*A*) passing through or next to the TbLRRP1 loop, which is in tight association with the FPC (*B* and *C*). In *A*, 5 cells were shown from *left* to *right*, representing cell cycle progress. In *B* and *C*, 3 cells (marked *1*, *2*, and *3*) were shown representing different cell cycle stages. The assembly of a new YFP-TbSpef1-containing structure (arrowhead) took place before kinetoplast division and FPC/bi-lobe segregation.

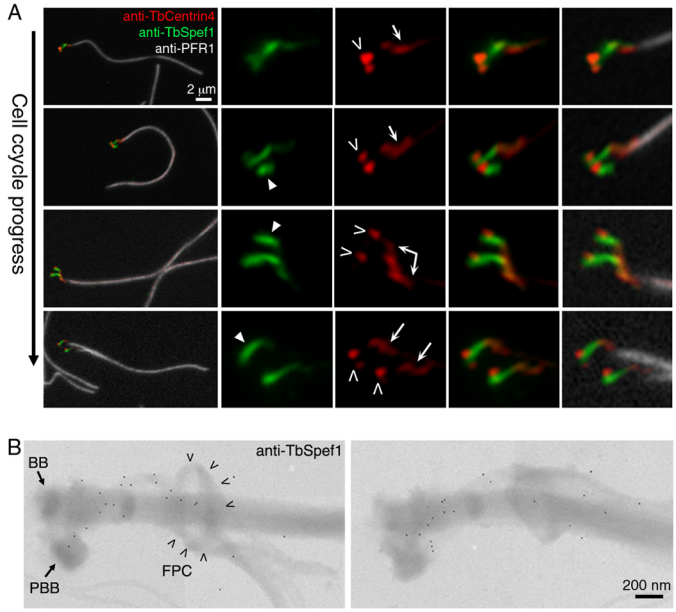

FIGURE 3. **TbSpef1 traces along the MtQ between the basal bodies and the FPC/bi-lobe.** *A*, 29.13 cells were extracted with 1% Nonidet P-40 and 1 M NaCl, fixed with PFA, and labeled with anti-TbSpef1 (*green*), anti-TbCentrin4 (*red*) for the basal bodies (*open arrowheads*) and bi-lobe (*arrows*), and anti-PFR1 for PFR (*gray*). Four cells representing cell cycle progress were shown from *top* to *bottom*. New TbSpef1-containing structure (*filled arrowheads*) was assembled before basal body and bi-lobe duplication. *B*, 29.13 cells were extracted with 1% Nonidet P-40 and 1 M NaCl and immunogold-labeled with anti-TbSpef1. Anti-TbSpef1 labeling was found along the MtQ segment in between the basal bodies (*BB*, mature basal body; *PBB*, pro-basal body) and the FPC (*open arrowheads*).

organelles including the basal bodies, the FPC, the bi-lobe, and the FAZ. Efficient TbSpef1 depletion was achieved by tetracycline-inducible RNAi (supplemental Fig. S4*B*), and cells depleted of TbSpef1 demonstrated motility defects as previously observed (data not shown). Cell proliferation slowed 24 h post-induction and completely halted 48 h post-induction (supplemental Fig. S4*A*). The accumulation of multinucleated cells also supported previous observations of cell division defects (supplemental Fig. S4C).

In *T. brucei*, single-copied organelles including basal bodies, kinetoplast, flagellum, FPC, bi-lobe, and FAZ all duplicate and segregate before nuclear division. We, therefore, chose to analyze the effects of TbSpef1-RNAi in post-mitotic cells (cells containing two divided nuclei) at 36 h post-TbSpef1-RNAi. At this time point, the percentage of abnormal post-mitotic cells peaked, and the percentage of multinucleated cells, akinetoplast cells, and zoids (cells lacking nucleus) were relatively low (supplemental Fig. S4C).

Three major types of post-mitotic cells were observed in the TbSpef1-RNAi population at 36 h post-induction. These included 1K2N cells with undivided kinetoplasts as well as 2K2N cells with normal kinetoplast positioning relative to the nuclei (KNKN) or abnormal kinetoplast arrangements (KKNN or NKKN). The kinetoplasts, although divided, remained close to each other in the KKNN and NKKN cells (Fig. 4, *A* and *B*). The accumulation of NKKN, KKNN, and 1K2N cells in the TbSpef1-depleted cells indicated an inhibition in kinetoplast segregation, consistent with the observation of duplicated but un-segregated basal bodies in these cells (Fig. 4*A*). Maturation of these basal bodies was also normal, as new flagellum biogenesis proceeded normally (Fig. 4, *B* and *C*). Depletion of TbSpef1 appeared not to affect new basal body migration during its maturation process (17). New flagellum was constructed posterior to the old flagellum in TbSpef1-depleted cells, as is the case in control parasites (supplemental Fig. S5). However, the assembly of a new MtQ appeared inhibited at the base of the new flagellum (supplemental Fig. S6). The lack of a new MtQ could

Downloaded from http://www.jbc.org/ at UNIV BORDEAUX on February 5, 2015

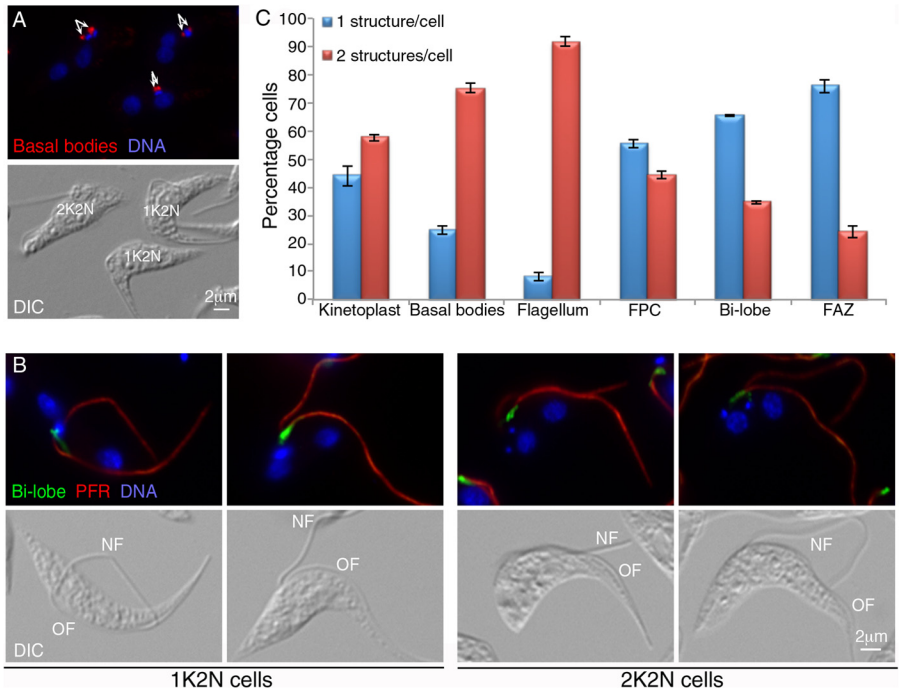

FIGURE 4. **TbSpef1-RNAi has distinct effects on the duplication of different organelles.** Cells induced for TbSpef1-RNAi for 36 h were fixed and labeled with YL1/2 for basal bodies (*red*, *arrows*) (*A*) or anti-TbLRRP1 for bi-lobe (*green*) and anti-PAR for PFR (*red*) (*B*). Duplication of subcellular structures was quantified in post-mitotic cells (*C*). 200 cells were counted in each of three independent experiments. Results were shown as the percentage cells ± S.D. In the absence of TbSpef1, duplication of the kinetoplast, basal bodies, and the flagella appeared normal, whereas duplication of the FPC, the bi-lobe, and the FAZ was inhibited. Basal bodies segregation, however, was inhibited, resulting in segregation defects of kinetoplasts and flagella. *NF*, new flagellum; *OF*, old flagellum.

explain the inhibited duplication of FPC, bi-lobe, and FAZ in these cells (Fig. 4, *B* and *C*). However, in some cases the single FPC or bi-lobe structure appeared larger and brighter, and it was possible that these represented duplicated but un-segregated structures (see Fig. 4*B*, *second panels from left*). Taken together, these results indicated a distinct effect of TbSpef1 on different organelles; whereas FPC, bi-lobe, and FAZ duplication was inhibited, basal bodies, kinetoplast, and flagellum could duplicate but failed to segregate.

p197, a TAC Protein—The product of Tb927.10.15750, an ~197 kDa protein, was previously identified as a basal body component in the flagellar complex proteome (23). A closer examination of p197, stably expressed as a YFP fusion from an endogenous allele, revealed a consistent localization of p197 between the kinetoplast DNA and the basal bodies labeled with YL1/2 (Fig. 5), and this was further confirmed by super-resolution microscopy using an ELYRA system (Fig. 5*B*). As basal bodies duplicated and moved apart, the YFP-p197 structure also duplicated and marked the outer edges of the dividing kinetoplast. Both the localization and the duplication pattern of the YFP-p197 structure were reminiscent of the TAC structure that mediates the physical connection between kinetoplast DNA and the basal bodies (15).

To examine if p197 indeed functioned as a TAC protein, p197 was depleted by tetracycline-inducible RNAi in procylic cells. Upon induction, cells grew normally for 3 days and then slowed down with a doubling time of ~48 h from day 3 to day 9 (Fig. 6*A*). Akinetoplast cells continued to accumulate, accounting for >90% of the p197-RNAi population at 4 days post induction (Fig. 6*A*). This was confirmed by staining the cells with DAPI that labeled both kinetoplast and nuclear DNA as well as dihydroethidium that selectively labeled kinetoplast DNA (38). Loss of the kinetoplast was likely due to asymmetrical kinetoplast inheritance, as cells with abnormally large or abnormally small kinetoplasts were frequently observed in the culture 1–3 days post-induction (Fig. 6*A*). Nuclear division and duplication/segregation of basal bodies and flagella in these cells appeared normal, and the large kinetoplast was found associated with only one of the duplicated basal bodies (Fig. 6*B*). The severed link between the kinetoplast and the basal bodies observed in p197-depleted cells recapitulated the RNAi effects of p166, a TAC component previously identified (16).

Interestingly, despite inhibited cell proliferation, the akinetoplast cells remained viable up to 10 days post p197-RNAi as shown by their apparently normal cell motility and membrane impermeability to nucleic acid dye propidium iodide (data not shown). Continued cultivation of p197-RNAi cells in the presence of tetracycline resulted in reversed RNAi phenotypes and at 14 days post-induction the culture was dominated with kinetoplast-containing cells that might have escaped the RNAi effect (data not shown).

FP45 Encircles the Flagellar Pocket—FP45 (encoded by Tb927.9.9730) is a 399-amino acid hypothetical protein containing two BRCA1 C terminus (BRCT) domains, one near the N terminus (amino acids 58–161) and the other near the C terminus (amino acids 266–376) (Fig. 7*A*). As the BRCT domain is found mainly in cell cycle checkpoint proteins responsive to DNA damage (39, 40), we decided to further examine the localization of FP45 in *T. brucei.* Procyclic cells with tetracycline-inducible expression of YFP-FP45 were monitored by fluorescence microscopy (Fig. 7*B*). YFP-FP45 was found in the region between the kinetoplast and the FPC.

Downloaded from http://www.jbc.org/ at UNIV BORDEAUX on February 5, 2015

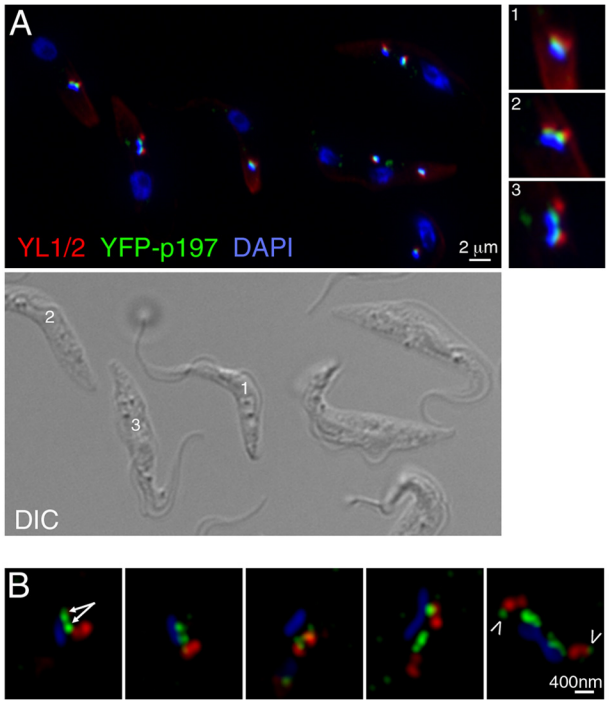

FIGURE 5. **p197 maps to a region between the basal bodies and the kinetoplast DNA.** Procyclic cells endogenously expressing YFP-p197 were fixed with PFA and labeled with anti-GFP (*green*), DAPI (*blue*), and YL1/2 for the basal bodies (*red*). The cells were then imaged with an epifluorescence microscope (*A*) and an ELYRA microscope for super-resolution images (*B*). Enlarged images of 3 cells (marked *1*, *2*, and *3*) representing different basal body duplication stages were shown on the *right* in *A*. YFP-p197 was localized to a region between the basal bodies and the kinetoplast, and the p197-containing structure was duplicated and segregated after the basal bodies. Super-resolution images suggested that p197 labeled a pair of dots (*arrows*) in close association with the kinetoplast DNA and at an angle to the mature basal bodies marked by *YL1/2*. As basal bodies and p197-containing structure duplicated and moved apart to divide the kinetoplast, extra p197 dots also appeared in close association with each of the duplicated basal bodies (*arrowheads*). Whether this represented newly formed TAC was not clear and they were not observed in the epifluorescence images.

Unlike TbSpef1 that was also found in this region, FP45 was a soluble protein and was efficiently extracted by detergent (Fig. 7*E*). The exact localization of YFP-FP45 was further examined by immuno-cryoEM with anti-GFP. The gold particles were found in the flagellar pocket region outlining the flagellar pocket membrane (Fig. 7, *F* and *G*).

A polyclonal antibody was raised against FP45 and used for immunofluorescence assays and immunoblotting of both procyclic and bloodstream form *T. brucei* cells. Both the endogenous FP45 and the YFP-FP45 were detected by the antibody on immunoblots as shown in Fig. 7*C*. Interestingly, whereas FP45 was expressed in both the bloodstream form and procyclic cells on immunoblots (Fig. 7*D*), immunolabeling of endogenous FP45 was observed only in the bloodstream form cells but not in the procyclic cells (Fig. 7*H* and data not shown). The flagellar pocket localization of FP45 in the bloodstream form cells was verified by co-localization with tomato-lectin. Despite many attempts, we were not able to generate stable RNAi cell lines that exhibited efficient FP45 depletion in either procyclic or bloodstream stage parasites.

DISCUSSION

Recent work on the bi-lobe revealed a remarkable structural and molecular complexity of this structure. In addition to TbCentrin2, the defining molecule of bi-lobe, several other proteins including TbCentrin4, TbPlk, TbMORN1, and TbLRRP1 were also found present or transiently associated with the structure. Characterization of these new markers not only attested the functional importance of the bi-lobe but also emphasized its multiplex nature and its tight association with other subcellular structures (9), which made previous purification attempts unsuccessful (23).

In search for new bi-lobe proteins and to understand its association with other structures, the bi-lobe was immunoisolated for proteomic analyses. Previous attempts to identify flagellum and bi-lobe proteins relied on detergent and high salt extractions of the parasite cells, which removed most of the soluble and membrane associated proteins and allowed characterization of only the core cytoskeletal components. The molecular association between the bi-lobe and membranous structures including the ER exit site/Golgi and the flagellar pocket remained elusive. Our current immunoisolation approach used a detergent-free isotonic buffer and enabled both soluble and structural proteins associated with the bi-lobe to be preserved during the purification steps and identified by mass spectrometry.

One of the soluble components identified in this study was FP45, a 45-kDa, BRCT domain-containing protein localizing to the flagellar pocket in both procyclic and bloodstream form cells. The association of FPC with bi-lobe was first observed by Morriswood *et al.* (22), where the bi-lobe marker TbMORN1 was found in tight association with the FPC marker BILBO1. How the soluble FP45 is associated with the bi-lobe or the flagellar pocket remained unclear. Unlike previously characterized flagellar pocket proteins (41), FP45 lacked signal peptide or membrane anchors. Despite several attempts, functional studies by RNAi were not successful in our current study. The interesting domain organization of FP45, particularly the BRCT domain mostly found in DNA repair proteins, warrants further functional studies of this protein by conditional knock-out and/or other methods.

Interestingly, several mitochondrial proteins and one ER protein TbBiP were also identified (supplemental Table S1). We could not rule out the possibility that the presence of these mitochondrial proteins was due to contamination of the immunoisolated bi-lobe fraction. However, bi-lobe association with the mitochondrion and ER was not surprising. The kinetoplast DNA resides in a special domain within the mitochondrion and is linked to the basal bodies through the trans-mitochondrial membrane TAC complex. FAZ-ER, a specialized ER domain subtending the FAZ filament and nucleating the ER exit site and the Golgi, is also in close association with the bi-lobe (29, 42). In addition to TbBiP, two other ER proteins were identified as low confidence hits in our bi-lobe proteome (data not shown). Characterization of these ER proteins identified in the bi-lobe fraction may provide further insights on how these membrane-bound organelles are tethered to the cytoskeletal elements.

Downloaded from http://www.jbc.org/ at UNIV BORDEAUX on February 5, 2015

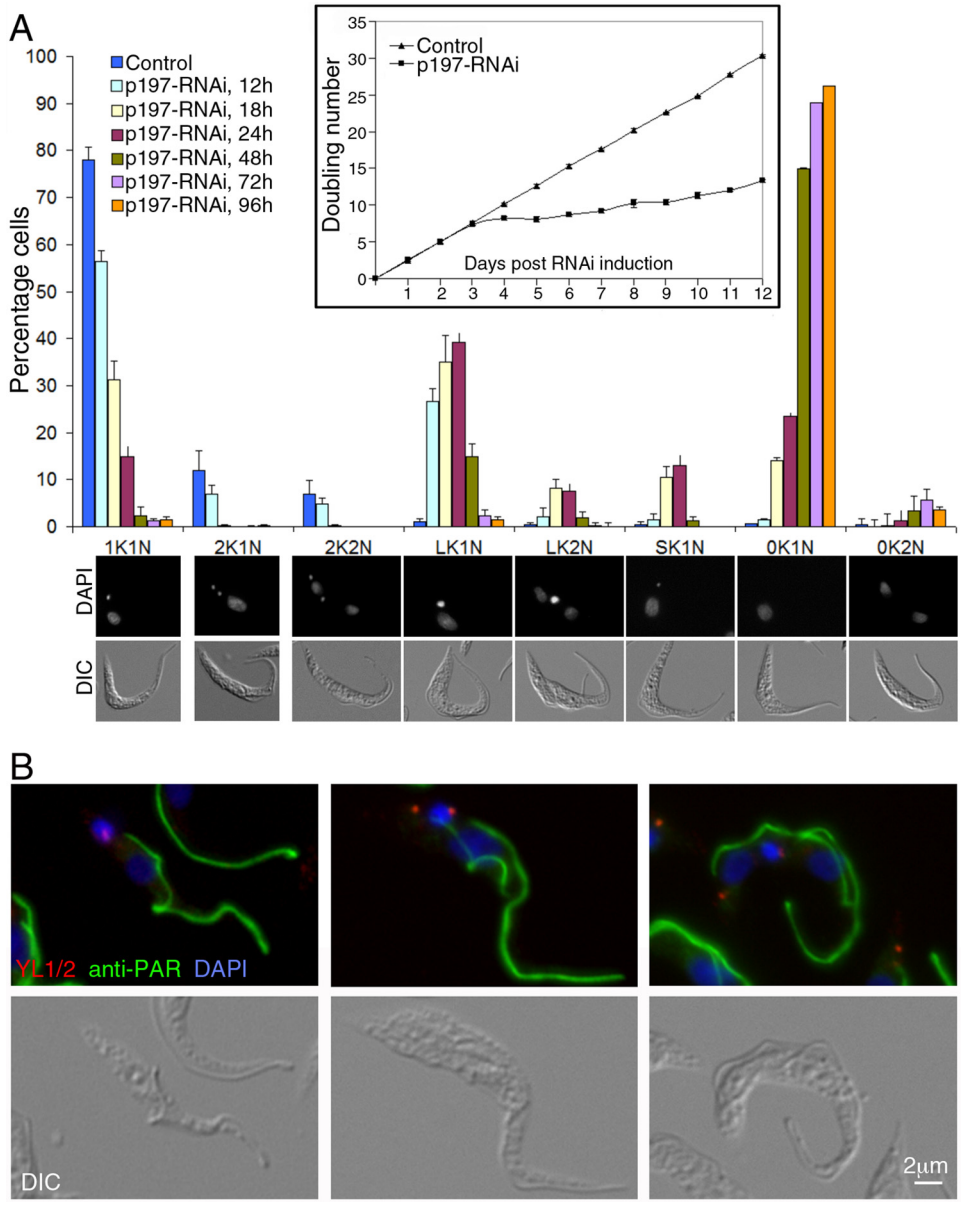

FIGURE 6. **p197-RNAi leads to unequal kinetoplast segregation.** Cells stably transfected for p197-RNAi were cultivated in the presence or absence of tetracycline. *A*, p197-RNAi cells induced for 12, 18, 24, 48, 72, and 96 h were monitored for kinetoplast and nuclear DNA contents. Un-induced p197-RNAi cells were used as control. 200 cells were counted at each time point in each of three independent assays, and the results are shown as the mean ± S.D. Shown at the *bottom* are representative images of cells belonging to each category. *Inset*, cell proliferation was monitored every day up to day 12 post-induction. Doubling number was obtained by $\log_2(Nt \times Df/N_0)$, where Nt was parasite concentration at a specific time point, N_0 was parasite concentration at $t = 0$, and Df was the cumulative dilution factor. Results were shown as the mean ± S.D. ($n = 3$). *B*, p197-RNAi cells induced for 24 h were fixed, permeabilized with methanol at −20 °C, and stained with YL1/2 for the basal bodies (*red*), anti-PAR for the PFR (*green*), and DAPI for DNA (*blue*). Duplication and segregation of the basal bodies and associated flagella appeared normal, but the large kinetoplast failed to segregate and remained associated with one of the basal bodies.

Three structural proteins were identified in the bi-lobe fraction: a 50-kDa basal body protein BB50, a TAC protein p197, and an Spef1-homolog previously considered as a flagellar protein. TbSpef1, by YFP tagging and antibody labeling, was localized to the proximal segment of the MtQ between the basal bodies and the FPC/bi-lobe complex, which duplicated very early in the cell cycle, before basal bodies duplication. The TbSpef1-labeled structure was thus named pMtQ, representing the proximal MtQ segment in between the basal bodies and the FPC/bi-lobe. Depletion of TbSpef1 inhibited new MtQ assembly and led to inhibited FPC, bi-lobe, and FAZ duplication. These effects may be due to inhibited *T. brucei* polo-like kinase (Plk) migration along the MtQ, which signals sequential organelle duplication during *T. brucei* cell cycle (43). On the contrary, duplication of the "upstream" organelles including the kinetoplast, the basal bodies, and the flagellum was not affected, although their segregation/division was greatly inhibited, likely due to the lack of new FAZ assembly in these cells (13). The lack of new FAZ assembly and subsequent flagellum detachment also explained the flagellum motility and cell division defects previously reported for TbSpef1-RNAi mutants (36, 37). It is worth noting that Spef1 homologues have also been found in various flagellated/ciliated organisms including *Chlamydomonas reinhardtii*, *Plasmodium falciparum*, *Drosophila*, and zebra

Downloaded from http://www.jbc.org/ at UNIV BORDEAUX on February 5, 2015

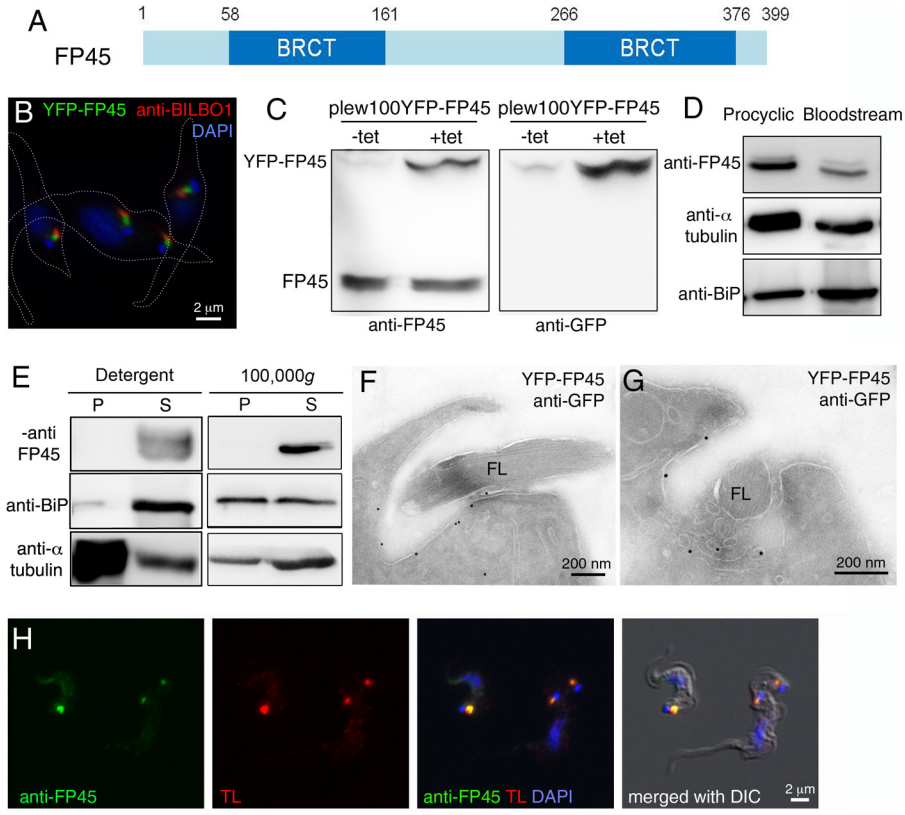

FIGURE 7. **FP45 is a soluble protein encircling the flagellar pocket.** *A*, domain organization of FP45 is shown. *B*, procyclic cells induced with tetracycline for YFP-FP45 overexpression (*green*) were fixed with methanol and labeled with anti-BILBO1 for the FPC (*red*) and DAPI for DNA (*blue*). Cell outlines were shown as *white dotted lines*. *C*, characterization of anti-FP45 is shown. Lysates of un-induced control or cells induced with tetracycline (*tet*) for YFP-FP45 expression were fractionated by SDS-PAGE and immunoblotted with anti-FP45 and anti-GFP. Anti-FP45 detected both the endogenous and YFP tagged FP45, whereas anti-GFP detected only the YFP-FP45. A weak band approximately the size of YFP-FP45 was detected in non-induced cells by both anti-FP45 and anti-GFP, possibly due to the un-regulated expression of YFP-FP45 in some cells. *D*, FP45 was expressed in both procyclic and bloodstream-form parasites. Lysates from 2.5×10^6 procyclic and 4.25×10^6 bloodstream form cells were fractionated by SDS-PAGE, and the blot was probed with a rat polyclonal anti-FP45. α-Tubulin and BiP were also probed as loading controls. *E*, FP45 is a soluble protein. 29.13 cells were extracted with 1% Nonidet P-40 in PBS followed by centrifugation at 6000 × *g* for 10 min to separate the detergent-soluble supernatant from the insoluble pellet. Alternatively, cells were sonicated, and cell lysates were centrifuged at 100,000 × *g* for 1 h. Equal fractions of pellet (*P*) and supernatant (*S*) were loaded on SDS-PAGE and immunoblotted with anti-FP45, anti-BiP, and anti-α-tubulin. FP45 was detected only in the supernatant under both conditions. ER luminal protein BiP and α-tubulin, used as the loading control, were found in both soluble and insoluble fractions. *F* and *G*, procyclic cells induced for YFP-FP45 overexpression were prepared for immunocryo-EM with anti-GFP. Gold particles representing FP45 localization were found at the flagellar pocket membrane. *FL*, flagellum. *H*, FP45 colocalized with tomato-lectin (*TL*) at the flagellar pocket in bloodstream-form cells. Cells were incubated with tomato lectin (*red*), fixed with PFA, and immunolabeled with anti-FP45 (*green*) and DAPI (*blue*).

fish as well as mammals (34). Cilia-associated microtubule structures similar to the MtQ, however, have not been observed in these organisms. In mouse testis, the Spef1 protein was localized to sperm tail, inside the fibrous sheath and around the outer dense fibers (34). Whether or not the Spef1 family proteins have the same cellular functions in different organisms remains to be investigated.

BB50 and p197 are indirectly associated with bi-lobe through their link with the basal bodies. The localization of p197 between the kinetoplast and the basal bodies and its RNAi phenotype both supported that it was a component of the TAC, which is a filamentous, trans-mitochondrial membrane complex linking the kinetoplast DNA to the basal bodies (15). Two TAC components, p166 and AEP1, have been identified before our current study (16, 44). Whereas both p166 and AEP1 have been shown to be mitochondrial proteins with transmembrane domains, p197 lacked predictable mitochondrial targeting signal or transmembrane domain. It is possible that p197 is present in the extra-mitochondrial domain of the TAC known as the exclusion zone filaments. Similar to p166, depletion of p197 severed the connection between the kinetoplast and the basal bodies, resulting in asymmetric kinetoplast division and accumulation of akinetoplast cells. Interestingly, without any detectable kinetoplast DNA, cells hardly proliferated, but their viability was not compromised. As mitochondrial function has been shown to be essential for procyclic cell survival (45), the mitochondrion or some mitochondrial functions may still be present in the akintoplast cells. The effects of kinetoplast depletion on mitochondrial function are under further investigation.

The characterization of BB50, p197, BILBO1, and TbSpef1 in the bi-lobe fraction further supported the bi-lobe association with other cytoskeletal structures including the basal bodies, the TAC, the FPC, and the FAZ microtubule quartet, although some of these associations may be indirect. These proteins provided useful new markers to visualize the duplication and segregation of these important cytoskeletal components during the cell cycle (Fig. 8). Organelle duplication started from the more posterior structures including the TbSpef1-containing pMtQ, the basal bodies, and the associated TAC and proceeded anterior to the FPC, the bi-lobe, and the FAZ filament. Disrup-

Downloaded from http://www.jbc.org/ at UNIV BORDEAUX on February 5, 2015

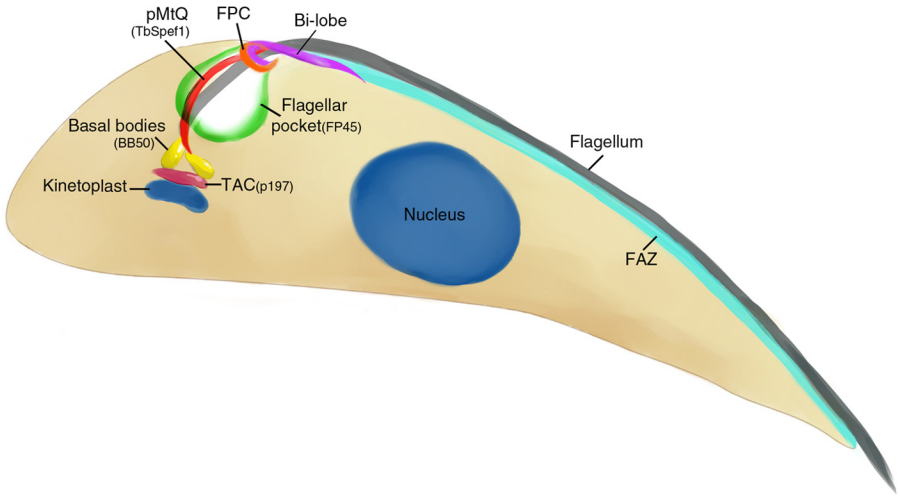

FIGURE 8. **A continuous cytoskeletal network tethers the basal bodies to the FPC/bi-lobe.** In this schematic view of a *T. brucei* cell, the relative localization of BB50, TbSpef1, p197, and FP45, all isolated as bi-lobe associated proteins, to other subcellular structures was shown. In the posterior region of the cell, a single kinetoplast was linked to the basal bodies, where BB50 was mapped. The kinetoplast DNA-basal body connection was mediated by TAC, which contained p166 and perhaps also p197. TbSpef1-containing pMtQ linked the basal bodies to the FPC and the bi-lobe. Attached to this cytoskeletal nexus were single-copied organelles including the kinetoplast, the flagellar pocket, the flagellum, and the FAZ.

tion of TbSpef1 function led to inhibited duplication of the organelles anterior to TbSpef1-labeled MtQ but not those posterior. Similarly, RNAi depletion of TbLRRP1, a bi-lobe marker, also led to inhibited duplication of the more anterior FAZ but not the duplication of the more posterior basal body-flagellum complex (23). Recent analyses on *T. brucei* polo-like kinase (Plk) localization throughout the cell cycle provided a mechanism where ordered movement of TbPlk along the FAZ MtQ to the FPC, the bi-lobe, and then the FAZ could signal the sequential duplication of these structures (43). As the cytoskeletal structures were undergoing duplication, other organelles including the kinetoplast, the flagellum, the flagellar pocket, Golgi/ER exit site, and FAZ-ER, which were attached to the core cytoskeletal network through different mechanisms, were also duplicated. Segregation of the cytoskeletal network thus mediated the segregation of these attached organelles. This sequential assembly of cytoskeletal elements along a continuous microtubule track together with associated membrane or non-membrane organelles provided an efficient strategy to ensure orderly inheritance of these single-copied organelles during the cell cycle. As new markers for the organelles and associated cytoskeletal elements became available, future work shall focus on detailing the order of assembly and the molecular mechanisms involved.

Acknowledgments—We thank Drs. Wang Chao and Y. Adam Yuan for help with expression of His-TbSpef1 and His-FP45 in E. coli, Dr. Wandy Beatty for immuno-cryoEM, Dr. Gang Dong for the anti-BILBO antibody, and Omar Sheriff for critical reading of the manuscript.

REFERENCES

1. Lowe, M., and Barr, F. A. (2007) Inheritance and biogenesis of organelles in the secretory pathway. *Nat. Rev. Mol. Cell Biol.* **8,** 429–439
2. Sheahan, M. B., Rose, R. J., and McCurdy, D. W. (2007) Mechanisms of organelle inheritance in dividing plant cells. *J. Integr. Plant Biol.* **49,** 1208–1218
3. Fagarasanu, A., and Rachubinski, R. A. (2007) Orchestrating organelle inheritance in *Saccharomyces cerevisiae*. *Curr. Opin. Microbiol.* **10,** 528–538
4. Imoto, Y., Yoshida, Y., Yagisawa, F., Kuroiwa, H., and Kuroiwa, T. (2011) The cell cycle, including the mitotic cycle and organelle division cycles, as revealed by cytological observations. *J. Electron Microsc.* **60,** S117–S136
5. Fagarasanu, A., Mast, F. D., Knoblach, B., and Rachubinski, R. A. (2010) Molecular mechanisms of organelle inheritance. Lessons from peroxisomes in yeast. *Nat. Rev. Mol. Cell Biol.* **11,** 644–654
6. Vickerman, K. (1969) On the surface coat and flagellar adhesion in trypanosomes. *J. Cell Sci.* **5,** 163–193
7. Woods, A., Sherwin, T., Sasse, R., MacRae, T. H., Baines, A. J., and Gull, K. (1989) Definition of individual components within the cytoskeleton of *Trypanosoma brucei* by a library of monoclonal antibodies. *J. Cell Sci.* **93,** 491–500
8. Sherwin, T., and Gull, K. (1989) The cell division cycle of *Trypanosoma brucei brucei*. Timing of event markers and cytoskeletal modulations. *Philos. Trans. R. Soc. Lond. B. Biol. Sci.* **323,** 573–588
9. Portman, N., and Gull, K. (2012) Proteomics and the *Trypanosoma brucei* cytoskeleton: advances and opportunities. *Parasitology* **139,** 1168–1177
10. García-Salcedo, J. A., Pérez-Morga, D., Gijón, P., Dilbeck, V., Pays, E., and Nolan, D. P. (2004) A differential role for actin during the life cycle of *Trypanosoma brucei*. *EMBO J.* **23,** 780–789
11. Nolan, D. P., and Garcia-Salcedo, J. A. (2008) Loss of actin does not affect export of newly synthesized proteins to the surface of *Trypanosoma brucei*. *Mol. Biochem. Parasitol.* **157,** 233–235
12. Absalon, S., Blisnick, T., Bonhivers, M., Kohl, L., Cayet, N., Toutirais, G., Buisson, J., Robinson, D., and Bastin, P. (2008) Flagellum elongation is required for correct structure, orientation, and function of the flagellar pocket in *Trypanosoma brucei*. *J. Cell Sci.* **121,** 3704–3716
13. Absalon, S., Kohl, L., Branche, C., Blisnick, T., Toutirais, G., Rusconi, F., Cosson, J., Bonhivers, M., Robinson, D., and Bastin, P. (2007) Basal body positioning is controlled by flagellum formation in *Trypanosoma brucei*. *PLoS One* **2,** e437
14. Robinson, D. R., and Gull, K. (1991) Basal body movements as a mechanism for mitochondrial genome segregation in the trypanosome cell cycle. *Nature* **352,** 731–733
15. Ogbadoyi, E. O., Robinson, D. R., and Gull, K. (2003) A high order transmembrane structural linkage is responsible for mitochondrial genome positioning and segregation by flagellar basal bodies in trypanosomes. *Mol. Biol. Cell* **14,** 1769–1779
16. Zhao, Z., Lindsay, M. E., Roy Chowdhury, A., Robinson, D. R., and Englund, P. T. (2008) p166, a link between the trypanosome mitochondrial

Downloaded from http://www.jbc.org/ at UNIV BORDEAUX on February 5, 2015

DNA and flagellum, mediates genome segregation. *EMBO J.* **27,** 143–154
17. Lacomble, S., Vaughan, S., Gadelha, C., Morphew, M. K., Shaw, M. K., McIntosh, J. R., and Gull, K. (2010) Basal body movements orchestrate membrane organelle division and cell morphogenesis in *Trypanosoma brucei*. *J. Cell Sci.* **123,** 2884–2891
18. He, C. Y., Ho, H. H., Malsam, J., Chalouni, C., West, C. M., Ullu, E., Toomre, D., and Warren, G. (2004) Golgi duplication in *Trypanosoma brucei*. *J. Cell Biol.* **165,** 313–321
19. Bonhivers, M., Nowacki, S., Landrein, N., and Robinson, D. R. (2008) Biogenesis of the trypanosome endo-exocytotic organelle is cytoskeleton-mediated. *PLoS Biol.* **6,** e105
20. He, C. Y., Pypaert, M., and Warren, G. (2005) Golgi duplication in *Trypanosoma brucei* requires Centrin2. *Science* **310,** 1196–1198
21. Shi, J., Franklin, J. B., Yelinek, J. T., Ebersberger, I., Warren, G., and He, C. Y. (2008) Centrin4 coordinates cell and nuclear division in *T. brucei*. *J. Cell Sci.* **121,** 3062–3070
22. Morriswood, B., He, C. Y., Sealey-Cardona, M., Yelinek, J., Pypaert, M., and Warren, G. (2009) The bilobe structure of *Trypanosoma brucei* contains a MORN-repeat protein. *Mol. Biochem. Parasitol.* **167,** 95–103
23. Zhou, Q., Gheiratmand, L., Chen, Y., Lim, T. K., Zhang, J., Li, S., Xia, N., Liu, B., Lin, Q., and He, C. Y. (2010) A comparative proteomic analysis reveals a new bi-lobe protein required for bi-lobe duplication and cell division in *Trypanosoma brucei*. *PLoS One* **5,** e9660
24. Esson, H. J., Morriswood, B., Yavuz, S., Vidilaseris, K., Dong, G., and Warren, G. (2012) Morphology of the trypanosome bilobe, a novel cytoskeletal structure. *Eukaryot. Cell* **11,** 761–772
25. Wirtz, E., Leal, S., Ochatt, C., and Cross, G. A. (1999) A tightly regulated inducible expression system for conditional gene knock-outs and dominant-negative genetics in *Trypanosoma brucei*. *Mol. Biochem. Parasitol.* **99,** 89–101
26. Bangs, J. D., Brouch, E. M., Ransom, D. M., and Roggy, J. L. (1996) A soluble secretory reporter system in *Trypanosoma brucei*. Studies on endoplasmic reticulum targeting. *J. Biol. Chem.* **271,** 18387–18393
27. Redmond, S., Vadivelu, J., and Field, M. C. (2003) RNAit: an automated web-based tool for the selection of RNAi targets in *Trypanosoma brucei*. *Mol. Biochem. Parasitol.* **128,** 115–118
28. Wang, Z., Morris, J. C., Drew, M. E., and Englund, P. T. (2000) Inhibition of *Trypanosoma brucei* gene expression by RNA interference using an integratable vector with opposing T7 promoters. *J. Biol. Chem.* **275,** 40174–40179
29. Zhou, Q., Liu, B., Sun, Y., and He, C. Y. (2011) A coiled-coil- and C2-domain-containing protein is required for FAZ assembly and cell morphology in *Trypanosoma brucei*. *J. Cell Sci.* **124,** 3848–3858
30. Kohl, L., Sherwin, T., and Gull, K. (1999) Assembly of the paraflagellar rod and the flagellum attachment zone complex during the *Trypanosoma brucei* cell cycle. *J. Eukaryot. Microbiol.* **46,** 105–109
31. Ismach, R., Cianci, C. M., Caulfield, J. P., Langer, P. J., Hein, A., and McMahon-Pratt, D. (1989) Flagellar membrane and paraxial rod proteins of *Leishmania*. Characterization employing monoclonal antibodies. *J. Protozool.* **36,** 617–624
32. Schlaeppi, K., Deflorin, J., and Seebeck, T. (1989) The major component of the paraflagellar rod of *Trypanosoma brucei* is a helical protein that is encoded by two identical, tandemly linked genes. *J. Cell Biol.* **109,** 1695–1709
33. Stephan, A., Vaughan, S., Shaw, M. K., Gull, K., and McKean, P. G. (2007) An essential quality control mechanism at the eukaryotic basal body prior to intraflagellar transport. *Traffic* **8,** 1323–1330
34. Chan, S. W., Fowler, K. J., Choo, K. H., and Kalitsis, P. (2005) Spef1, a conserved novel testis protein found in mouse sperm flagella. *Gene* **353,** 189–199
35. Dougherty, G. W., Adler, H. J., Rzadzinska, A., Gimona, M., Tomita, Y., Lattig, M. C., Jr., and Kachar, B. (2005) CLAMP, a novel microtubule-associated protein with EB-type calponin homology. *Cell Motil. Cytoskel.* **62,** 141–156
36. Baron, D. M., Ralston, K. S., Kabututu, Z. P., and Hill, K. L. (2007) Functional genomics in *Trypanosoma brucei* identifies evolutionarily conserved components of motile flagella. *J. Cell Sci.* **120,** 478–491
37. Broadhead, R., Dawe, H. R., Farr, H., Griffiths, S., Hart, S. R., Portman, N., Shaw, M. K., Ginger, M. L., Gaskell, S. J., McKean, P. G., and Gull, K. (2006) Flagellar motility is required for the viability of the bloodstream trypanosome. *Nature* **440,** 224–227
38. Wang, Z., Drew, M. E., Morris, J. C., and Englund, P. T. (2002) Asymmetrical division of the kinetoplast DNA network of the trypanosome. *EMBO J.* **21,** 4998–5005
39. Callebaut, I., and Mornon, J. P. (1997) From BRCA1 to RAP1. a widespread BRCT module closely associated with DNA repair. *FEBS Lett.* **400,** 25–30
40. Bork, P., Hofmann, K., Bucher, P., Neuwald, A. F., Altschul, S. F., and Koonin, E. V. (1997) A superfamily of conserved domains in DNA damage-responsive cell cycle checkpoint proteins. *FASEB J.* **11,** 68–76
41. Field, M. C., and Carrington, M. (2009) The trypanosome flagellar pocket. *Nat. Rev. Microbiol.* **7,** 775–786
42. Bangs, J. D. (2011) Replication of the ERES:Golgi junction in bloodstream-form African trypanosomes. *Mol. Microbiol.* **82,** 1433–1443
43. Ikeda, K. N., and de Graffenried, C. L. (2012) Polo-like kinase is necessary for flagellum inheritance in Trypanosoma brucei. *J. Cell Sci.* **125,** 3173–3184
44. Ochsenreiter, T., Anderson, S., Wood, Z. A., and Hajduk, S. L. (2008) Alternative RNA editing produces a novel protein involved in mitochondrial DNA maintenance in trypanosomes. *Mol. Cell. Biol.* **28,** 5595–5604
45. Stephens, J. L., Lee, S. H., Paul, K. S., and Englund, P. T. (2007) Mitochondrial fatty acid synthesis in *Trypanosoma brucei*. *J. Biol. Chem.* **282,** 4427–4436

Downloaded from http://www.jbc.org/ at UNIV BORDEAUX on February 5, 2015